Propagation of premixed flames in the presence of Darrieus-Landau and Thermal Diffusive instabilities

Francesco Creta[a,*], Pasquale Eduardo Lapenna[a], Rachele Lamioni[a], Navin Fogla[b], Moshe Matalon[c]

[a] *Dept. of Mechanical and Aerospace Engineering, Sapienza University of Rome, Italy*
[b] *Gamma Technologies, Westmont, IL 60559*
[c] *Mechanical Science and Engineering, University of Illinois at Urbana-Champaign, Urbana, IL. 61801*

Abstract

We study the propagation of premixed flames, in the absence of external turbulence, under the effect of both hydrodynamic (Darrieus-Landau) and thermodiffusive instabilities. The Sivashinsky equation in a suitable parameter space is initially utilized to parametrically investigate the flame propagation speed under the potential action of both kinds of instability. An adequate variable transformation shows that the propagation speed can collapse on a universal scaling law as a function of a parameter related to the number of unstable wavelengths within the domain n_c. To assess whether this picture can persist in realistic flames, a DNS database of large scale, two-dimensional flames is presented, embracing a range of n_c values and subject to either purely hydrodynamic instability (DL) or both kinds of instability (TD). With the aid of similar DNS databases from the literature we observe that when adequately rescaled, propagation speeds follow two distinct scaling laws, depending on the presence of thermodiffusive instability or lack thereof. We verify the presence of secondary cutoff values for n_c identifying (a) the insurgence of secondary wrinkling in purely hydrodynamically unstable flames and (b) the attainment

*Corresponding author.
Email addresses: francesco.creta@uniroma1.it (Francesco Creta), pasquale.lapenna@uniroma1.it (Pasquale Eduardo Lapenna), rachele.lamioni@uniroma1.it (Rachele Lamioni), n.fogla@gtisoft.com (Navin Fogla), matalon@illinois.edu (Moshe Matalon)

of domain independence in thermodiffusively unstable flames. A possible flame surface density based model for the subgrid wrinkling is also proposed.
Keywords: premixed flames; hydrodynamic instability; thermal diffusive instability; Sivashinsky equation; Direct Numerical Simulation; self-turbulent flames

1. Introduction

Premixed flame propagation can be affected by exogenous phenomena such as turbulence as well as by endogenous effects such as intrinsic flame instabilities and, indeed, by the non-trivial, synergistic action of both [1, 2, 3, 4]. While the effects of turbulence on flame morphology, transport and characterization of turbulent speed have received universal attention trough theoretical, numerical and experimental studies [5, 6, 7, 8, 9], the specific role of intrinsic instabilities has only recently gained increasing interest. Various experimental [10, 11, 12, 13, 14, 3], analytical [4, 15] and numerical [16, 17, 18, 19, 2, 20] studies have indeed shown that instabilities can play a substantial role in flame propagation, especially at low turbulence intensity. On a practical level, intrinsic intabilities may be key in understanding such phenomena as accidental large scale gas explosions [21] or in explaining the effects of pressure on flame propagation [3, 22] or in accounting for the inaccuracy of sub-grid modelling in numerical simulations of premixed turbulent combustion [23], to name a few examples. In all cases, instabilities will tend to dramatically corrugate the flame surface, according to morphological features that can enhance the flame propagation and whose characteristics need to be accurately studied if a full understanding of the propagative behavior is to be acquired.

Flame instabilities are activated by two distinct mechanisms: the ubiquitous Darrieus-Landau (or hydrodynamic) mechanism, due to thermal expansion, which is therefore unconditionally active, and by thermal diffusive destabilizing effects which are generally manifested as small scale corrugation for sub-unity Lewis number conditions. The latter are dictated by the mass diffusivity of

the controlling reactant, such as those encountered in lean hydrogen [24] or hydrogen-diluted mixtures [25]. Whether thermal diffusive effects are stabilizing or destabilizing, a cutoff wavelength λ_c exists, depending on the mixture and on pressure, for which all perturbations of larger wavelength will destabilize an unconstrained planar front. Such cutoff wavelength can be estimated to be one to two orders of magnitude larger than the flame thickness [2, 16, 26, 27] thereby rendering instability effects inherently large-scale in nature, i.e. visible only for unconstrained flames, spherical expanding flames, large enough Bunsen or slot flames etc. Indeed, the large scale nature of such phenomena and the ensuing potentially vast scale separation this entails [16], is the root cause hindering realistic three-dimensional direct numerical simulations of intrinsically unstable flames encompassing domains which are e.g. one or more orders of magnitude larger than the cutoff wavelength. This was accomplished only using simpler tools, such as weakly nonlinear flame models [1, 28] or in two-dimensional domains [17, 18] where, under certain conditions, flames were shown to exhibit a fractal conformation [17, 28].

The occurrence of intrinsic flame instabilities depends ultimately on the cutoff wavelength and how this compares to a characteristic hydrodynamic length scale L constraining the premixed flame, such as e.g. a Bunsen diameter or the radius of an expanding spherical flame. Any small scale flame for which $L < \lambda_c$ will therefore inhibit intrinsic instabilities. On the other hand, when $L > \lambda_c$, cellular corrugation will invariably manifest itself due to either purely hydrodynamic effects, when $Le > Le_0$ or due to the interplay of both hydrodynamic and thermal diffusive effects, when $Le < Le_0$, where $Le_0 \lesssim 1$ is a critical Lewis number. Given the complex and diverse nature of instability effects, an important preliminary task is therefore the identification of a minimum set of parameters which uniquely and unambiguously identify such effects. This is a first step towards the identification of universal scaling laws formulated as a function of such parameters. The primary objective of this work is to extend the findings of previous work [1], which was limited to the effect of Darrieus-Landau instability, by incorporating thermal-diffusive effects and do so in a laminar setting. The

interplay of such effects with turbulence and the implications this may have on scaling laws and on possible modifications of existing premixed turbulent combustion models is left to a future study. As mentioned, we therefore identify the most suitable set of independent parameters and subsequently verify if observables, such as the global propagation speed of the corrugated flame front, obey universal scaling laws in terms of such parameters.

This work is divided into two parts. The first part utilizes the weakly nonlinear Sivashinky model [29] to approach the general problem of the interplay between hydrodynamic and thermal diffusive instability in a freely propagating flame front in the absence of external turbulence. Independent parameters are identified and a universal scaling law for the propagation speed is formulated. Drawing on the findings of the first part and abandoning the constraining hypotheses of the Sivashinky model, the second part uses direct numerical simulations (DNS) of large scale two-dimensional unstable flames to construct a database which, in conjunction with other existing DNS databases, is used to formulate scaling laws which extend their validity to more realistic fully nonlinear regimes.

2. The Sivashinsky model

In this section we summarize the weakly nonlinear flame model, as first introduced by Sivashinky [29] as well as its equivalent forms, obtainable through transformation of variables. The associated dispersion relations, as well as more elaborate dispersion relations resulting from hydrodynamic theory, are then used as a guide to establish the stability characteristics as a function of the model parameters. Solutions of the ~~generalized~~ Sivashinky model are later used to determine a scaling law for the front propagation speed.

2.1. Model definition and linear stability

The weakly nonlinear integro-differential Sivashinsky equation [29] describes the evolution of the perturbation of a planar flame front and accounts for both

thermal-diffusive and hydrodynamic effects. In its most general form it reads as follows

$$F_t + 4(1+\epsilon)^2 F_{xxxx} + \epsilon F_{xx} + \frac{1}{2}F_x^2 = (1-\sigma)I(F) \tag{1}$$

where

$$I(F) = \frac{1}{4\pi}\int_{-\infty}^{\infty}\int_{-\infty}^{\infty} |k| F(\tilde{x},t) e^{ik(x-\tilde{x})} dk d\tilde{x}$$

and where $F(x,t)$ is the dimensionless flame perturbation, considered as a single-valued function of the dimensionless coordinate x, both measured in units of the flame thickness l_f. $\sigma = \rho_b/\rho_u < 1$ is the ratio of burned to unburned density (coefficient of thermal expansion) and $\epsilon = (Le_0 - Le)/(1 - Le_0)$, where Le is the Lewis number of the deficient reactant and $Le_0 < 1$ is a critical Lewis number. Dimensionless time t is measured in units of l_f/S_L where S_L is the velocity of the planar laminar flame. Note that Eq.(1) was obtained by assuming that (i) $Le \sim Le_0 < 1$ (ii) thermal expansion is weak $1-\sigma << 1$ (iii) the nondimensional activation energy $N = E/RT_b$ is a large number (using the notation used in [29]). A mathematically more systematic derivation given later by Sivashinsky [30] considering the distinguished limit $N(1-Le) = O(1)$, led to an equation similar to (1) but with the coefficient $(1+\epsilon)^2 \approx 1$. Since, as explained below, we intend to accept the Sivashinsky model without any restriction on the Lewis number Le (or equivalently on ϵ), the original form (1) will be retained in the following discussion.

Equation (1) accounts for the coexistence of thermal-diffusive and thermal expansion effects on the stability and propagation of a premixed flame. The second, third and fourth terms on the left hand side represent respectively a short wavelength stabilization term, a term accounting for stabilizing/destabilizing thermal-diffusive effects, depending on whether Le is above/below Le_0, or ϵ is negative/positive respectively, and a nonlinear front propagation term. The right hand side, on the other hand, accounts for the destabilizing effect of thermal expansion. The dispersion relation associated to the linearized form of Eq. (1), expressing the growth rate ω of a perturbed flame front with perturba-

tion of wavenumber k, reads

$$\omega = (1/2)(1-\sigma)k + \epsilon k^2 - 4(1+\epsilon)^2 k^4, \tag{2}$$

indicating the unconditionally unstable character of the hydrodynamic (Darrieus-Landau) term due to thermal expansion (first term on the right hand side), the stabilizing/destabilizing diffusive effect (second term) depending on whether $\epsilon < 0$ or $\epsilon > 0$ respectively and the stabilizing fourth order term. Note that when $\epsilon > 0$ ($Le < Le_0$), i.e. destabilizing thermal-diffusive effects and in the absence of hydrodynamic effects, $\sigma = 1$ (constant density), Eq. (1) reduces to a form of the Kuramoto-Sivashinsky (KS) equation [30, 31] which can lead to complex small-scale cellular structures and chaotic dynamics. On the other hand when $\epsilon = -1$ and $\sigma \neq 1$, instabilities of thermal-diffusive origin are not present and the flame is only subject to hydrodynamic effects. In this latter case Eq. (1) can be recast into the Michelson-Sivashinsky (MS) form [32, 33, 34, 35, 1] by adopting the following variable transformation

$$F = (1-\sigma)^{2/3} u \;\; ; \;\; t = (1-\sigma)^{-4/3}\tau \;\; ; \;\; x = (1-\sigma)^{-1/3}\xi \tag{3}$$

which yields the MS form

$$u_\tau - \alpha\, u_{\xi\xi} + \frac{1}{2}u_\xi^2 = I(u) \;\; ; \;\; \alpha = (1-\sigma)^{-2/3} \tag{4}$$

In particular, Eq. (4), which possesses analytical "pole" solutions [36], was extensively analyzed in a previous study by Creta et al. [1] both in its original laminar form and in a forced version in which a correlated noise term was added to mimick turbulent motions.

Although the Sivashinsky equation (1) is valid in a small neighborhood of Le_0 and for small thermal expansion, for illustrative purposes it will be used, in this context, as a generalized equation even beyond its region of validity in order to fully capture the qualitative effect of parameter variation on the flame. For example, in the range $\epsilon < 0$ we will at times assume $|\epsilon|$ large enough so that $Le > 1$ values will be considered in the analysis or $1-\sigma$ large enough to encompass more realistic thermal expansion values.

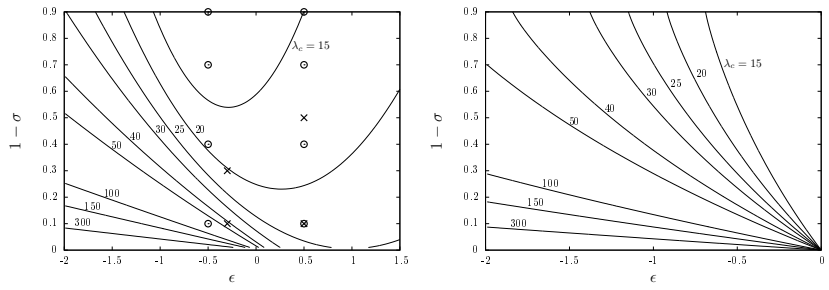

(a) λ_c Sivashinsky model Eq. 2 (b) λ_c MCB model Eq. 8

Figure 1: Critical wavelength λ_c shown on the $(\epsilon, 1-\sigma)$ plane for (a) dispersion relation Eq. 2 relative to Sivashinsky model Eq. 1 and (b) as estimated via the MCB model Eq. 8 with $Ze = 9$. Symbols correspond to solutions shown in Fig. 4 for 1D flames ($\circ$) and in Fig. 5 for 2D flames ($\times$).

The dispersion relation Eq. 2 yields a critical (cutoff) wavenumber k_c and a critical wavelength $\lambda_c = 2\pi/k_c$, obtained by imposing $\omega = 0$. Figure 1(a) displays λ_c on the parameter plane (ϵ,$1-\sigma$). Considering any contour line in Figure 1(a) as representative of domain size L, then all values of ϵ and σ that lie above such line will trigger instabilities because $L > \lambda_c$, while all values below this line will yield stable flames since $L < \lambda_c$. A domain size of $L = 400$ units of flame thickness, for example, is sufficient to trigger instabilities for almost all combinations of parameters ϵ and σ.

In the work by Michelson and Sivashinsky [37], for the case $\sigma \neq 1$ and $\epsilon \neq -1$, equation (1) was rescaled and presented in a one parameter form. The equation thus obtained reads

$$u_\tau + u_{\xi\xi\xi\xi} + \beta u_{\xi\xi} + \frac{1}{2}u_\xi^2 = I(u) \tag{5}$$

with the variable transformation given by

$$\begin{aligned} \beta &= 4^{-1/3}(1-\sigma)^{-2/3}\epsilon(1+\epsilon)^{-2/3}\,, \\ F &= u\epsilon/\beta\,,\ t = \tau\epsilon/[\beta(1-\sigma)^2]\,,\ x = \xi\epsilon/[\beta(1-\sigma)]. \end{aligned} \tag{6}$$

Figure 2(a) displays the parameter β on the (ϵ,$1-\sigma$) plane, thus relating the model represented by Eq. 5 to the original model Eq. 1. Such figure reveals

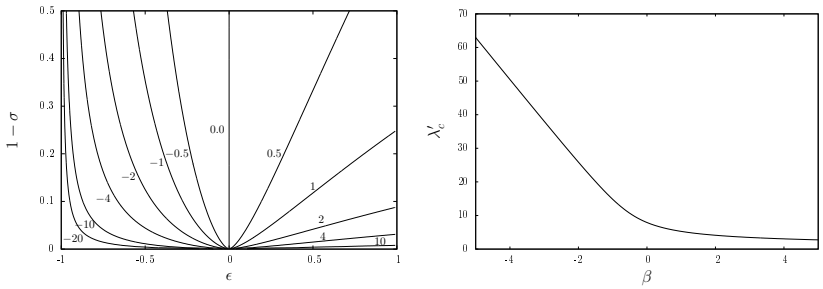

(a) parameter β (b) critical wavelength λ_c'

Figure 2: (a) Contour plot of the parameter β (Eq. (6)) on the (ϵ,$1-\sigma$) plane. (b) Critical wavelength λ_c' associated to Eq. (5).

that as $\beta \to \infty$, the model will only retain destabilizing thermodiffusive effects as $\epsilon > 0$ and $\sigma \to 1$. On the other hand, for $\beta < 0$, thermodiffusive effects will be stabilizing ($\epsilon < 0$) and, for a given ϵ, hydrodynamic effects will be stronger as $\beta \to 0$. The limiting case of $\beta \to -\infty$ corresponds to the model Eq. 4. The dispersion relation associated to the linearized form of equation (5) reads

$$\omega' = \frac{1}{2}k' + \beta k'^2 - k'^4. \tag{7}$$

The cutoff wavenumber k_c' of Eq. 7 and the corresponding critical wavelength $\lambda_c' = 2\pi/k_c'$ is displayed on Fig. 2(b) as a function of the parameter β. Note that according to the scaling Eq. (6) the critical wavelength corresponding to the original form given in Eq. (1) is recovered as the rescaled quantity $\lambda_c = \lambda_c'\epsilon/\beta(1-\sigma)$.

To incorporate the effects of realistic density ratios, we resort to the asymptotic dispersion relation that exploits the disparity between the hydrodynamic and diffusion scales, assuming that $\delta = l_f/L \ll 1$ where L is the the domain size, or hydrodynamic length. This expression, in dimensionless form, reads

$$\omega = \omega_0 k - \delta\left[B_1 + Ze(Le-1)B_2 + PrB_3\right]k^2 \tag{8}$$

where L is used as a unit of length and the laminar flame speed as a unit of velocity, and Ze, Pr and Le are the Zel'dovich, Prandtl and Lewis numbers,

respectively. Such expression was taken from [38], but was first derived in [39] by neglecting buoyancy and expanding the expression for the growth rate in powers of k. Parameters ω_0, $B_{1,2,3}$ are all functions of the expansion coefficient once the dependence of the transport coefficients on temperature, $\lambda(T)$, is specified. These expressions are properly listed in [40, 41] for a general $\lambda(T)$; in [38] they are presented only for $\lambda(T) = T$ (with a minor typo in B_2; the factor $\sigma - 1$ must be omitted). Note that in [38, 40, 41], σ is defined as the ratio of the unburned-to-burned density ratio, i.e., the inverse of the present definition. When the viscosity is assumed constant and independent of temperature one obtains $B_3 = 0$. By placing $\omega = 0$ one obtains the critical wavelength $\lambda_c = 2\pi/k_c$ which can be expressed in units of the flame thickness, similar to Fig.1(a), as λ_c/δ. In order to recast the result in a $(\epsilon, 1-\sigma)$ plane, Le_0 is recovered as the value for which the diffusive coefficient of the quadratic term in Eq. 8 changes sign, i.e.

$$Le_0 = 1 - \frac{B_1 + PrB_3}{ZeB_2} \tag{9}$$

The result for temperature independent transport coefficients is shown in Fig.1(b) where the domain is only limited to the $\epsilon < 0$, i.e. $Le > Le_0$, for which diffusive effects are stabilizing (i.e. the diffusive coefficient of the quadratic term in Eq. 8 is positive). Indeed, for $Le < Le_0$ Eq. 8 would diverge and a stabilization term would have to be sought by carrying the linear stability analysis to higher order, which has not been done in the literature. For $Le < Le_0$, however, we note a close qualitative similarity to results obtained via Eq. (5) and displayed in Fig. 1(a). The critical Lewis number Le_0 as a function of $1-\sigma$ is displayed in Fig. 3(b) for various values of Ze. Figure 3(a), following the definition of parameter ϵ, displays the Le field in the $(\epsilon, 1-\sigma)$ plane, where $Le = Le_0 - \epsilon(1 - Le_0)$.

2.2. Nonlinear evolution and front morphology

Representative solutions of Eq. 1 are displayed in Fig. 4 for a domain size $L = 400$, with periodic boundary conditions. Note that both the flame displacement $F(x,t)$ and domain size were rescaled according to Eq. (6). The left column,

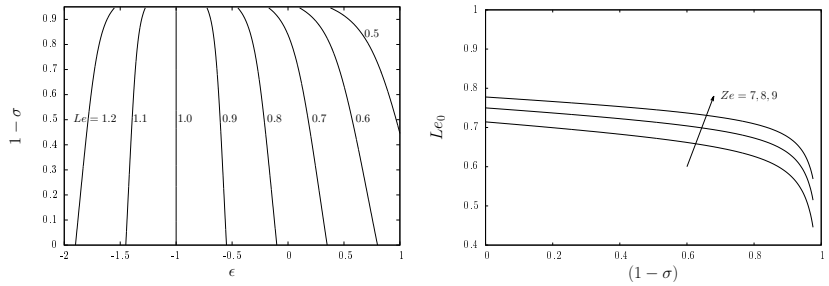

(a) Lewis number Le (b) critical Lewis number Le_0

Figure 3: (a) Contour plot of Le on the $(\epsilon, 1-\sigma)$ plane.. (b) Critical Le_0 as derived from Eq.9 with $Ze = 9$.

Fig. 4(a), represents $\epsilon < 0$ solutions for which only Darrieus-Landau effects are present, whereas the right column, Fig. 4(b), represents $\epsilon > 0$ solutions for which the additional thermal-diffusive instability is active. Solutions are displayed for growing values of $1-\sigma$. As can be observed in Fig. 4(a), Darrieus-Landau effects show as large scale (cusp-like) cells which are steadily propagating density ratios near unity. The effect of growing thermal expansion is to increase the amplitude of the cells. At high values of $1-\sigma$, a secondary unsteady corrugation appears, which disrupts the otherwise steady character of the large, cusp-like cells. Figure 4(b) shows how thermal-diffusive effects are manifested as a small scale unsteady corrugation which is superimposed on Darrieus-Landau cells. Clearly, one of the main limitations of the model is the single valued nature of the flame displacement $F(x,t)$, which does not allow for fold or pockets which are, however, basic characteristics of thermodiffusively unstable flames, as will be shown later in the DNS simulations.

Figure 5 shows similar solutions for the multidimensional version of Eq. 1. Very similar observations can be made for such two-dimensional flame surfaces, with the addition that the coupling of the corrugation in the two spatial dimensions gives rise to complex polyhedral structures, resembling caustic surfaces. Such structures are particularly evident in Fig. 6 in terms of curvature signatures, revealing the typically small scale corrugation in thermodiffusively

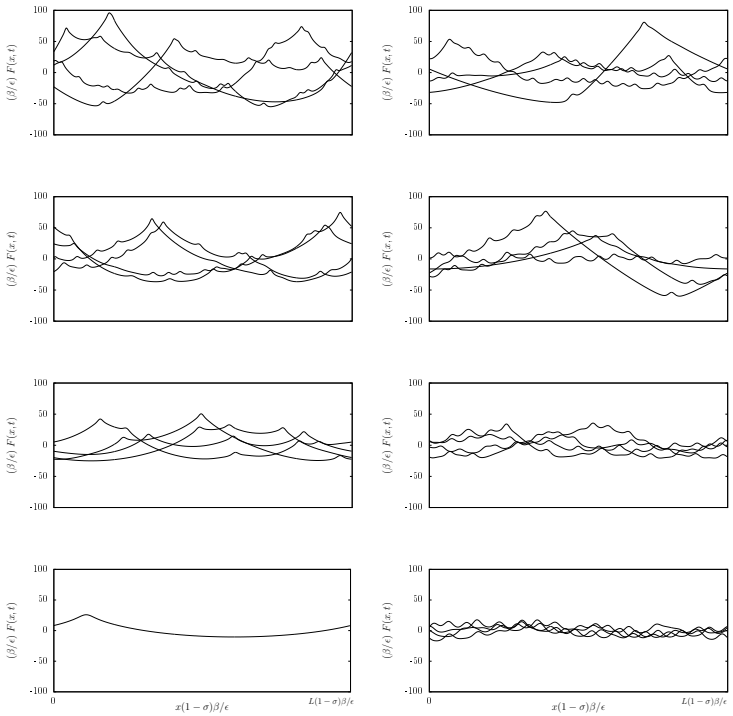

(a) $\epsilon = -0.5$ (b) $\epsilon = 0.5$

Figure 4: Solutions $F(x,t)$ of the one-dimensional Eq. 1 in a domain of size $L = 400$. Solutions and domain were rescaled according to Eq. (6). Left column (a) $\epsilon = -0.5$, right column (b) $\epsilon = 0.5$. From bottom to top figures: $\sigma = 0.9, 0.6, 0.3, 0.1$. From bottom to top: (a) $\beta = -2.32, -0.92, -0.63, -0.53$ (b) $\beta = 1.11, 0.44, 0.3, 0.26$.

unstable flames.

2.3. Front propagation velocity

The solution to Eq. (1) may be expressed at a given time as a corrugated profile propagating in the vertical y-direction, $F(x,t) = -Ut + \phi(x)$, where U, for steadily propagating structures, represents the incremental increase in propagation speed, in units of laminar flame speed, relative to a nominal laminar planar flame [1] and ϕ is a zero-mean perturbation of such planar flame. Substituting into Eq. (1) and taking the spatial average $\langle\cdot\rangle = (1/L)\int_0^L \cdot\, dx$, it

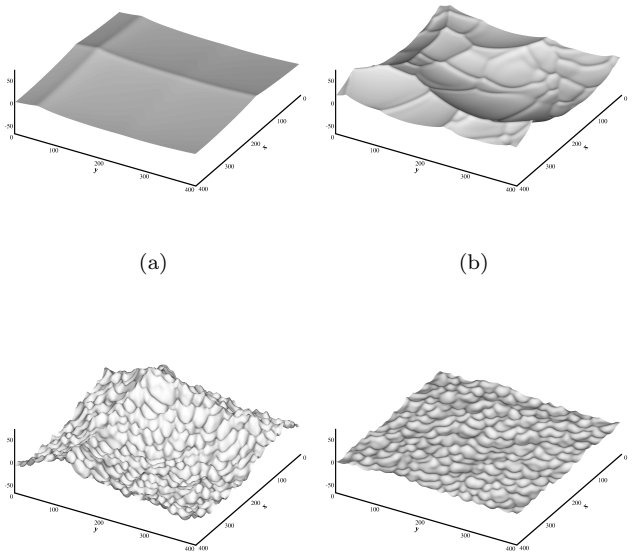

(a) (b)

(c) (d)

Figure 5: Solutions $F(x, y, t)$ of the two-dimensional form of Eq. 1 in a square domain of size $L = 400$ and for the following parameters (a) $\epsilon = -0.3$, $\sigma = 0.9$ ($\beta \approx -1.1$) (b) $\epsilon = -0.3$, $\sigma = 0.7$ ($\beta \approx -0.53$) (c) $\epsilon = 0.5$, $\sigma = 0.5$ ($\beta \approx 0.53$) (d) $\epsilon = 0.5$, $\sigma = 0.9$ ($\beta \approx 1.1$)

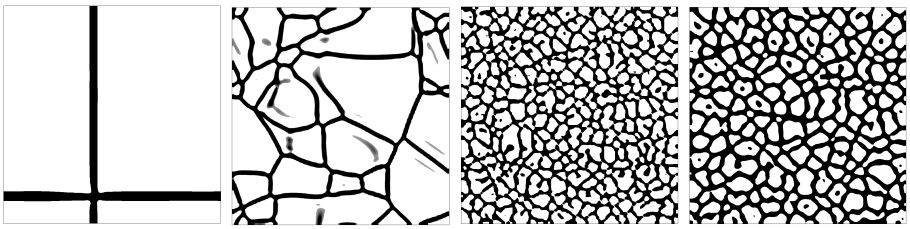

(a) (b) (c) (d)

Figure 6: Cellular structure of solutions displayed in Fig. 5 highlighed (black) in terms of the locus of negative curvature.

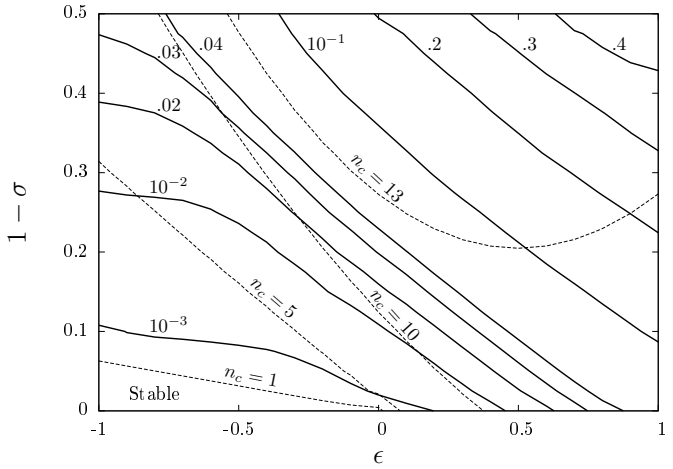

Figure 7: Contour plot on the $(\epsilon, 1-\sigma)$ plane of the mean incremental propagation speed $\overline{U}$ (bold continuous lines) for solutions to Eq.(1) on a domain of length $L = 400$. Also shown, the number of unstable cells $n_c = L/\lambda_c$ (dashed lines). Area below $n_c = 1$ ($L = \lambda_c$) is the parameter space region of stability.

can be shown, by enforcing continuity of derivatives at the periodic boundaries, that $U = (1/2)\langle(\phi_y(x))^2\rangle$. For unsteady cellular solutions, the time averaged incremental speed $\overline{U}$ acquires the meaning of an incremental speed of a (self-) turbulent front in statistical steady state, relative to the planar conformation.

A parametric campaign was performed by varying the parameters $(\epsilon, 1-\sigma)$ and seeking in turn statistically steady solutions of Eq. (1) on a domain of size $L = 400$ units of flame thickness. Figure 7 displays a plot of the mean incremental propagation speed $\overline{U}$ in the parameter plane $(\epsilon, 1-\sigma)$ for said solutions. We observe that the highest values of $\overline{U}$ occur for strong thermal expansion and large positive values of ϵ where the hydrodynamically unstable structure coexists with the thermodiffusively unstable cellular structure, thus enhancing the corrugated nature of the front. Figure 7 also displays the loci of constant number of unstable cells n_c which seems to correlate directly to $\overline{U}$.

Using the scaling in Eq. (6), the propagation speed data presented in Fig. 7 can be collapsed onto a single curve as a function of β, as shown in Fig. 8. The figure displays the scaled propagation speed $U/(1-\sigma)^2$ (here U is used

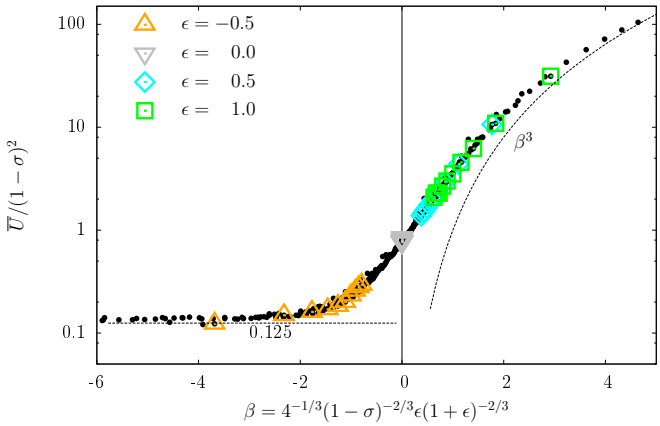

Figure 8: Rescaled propagation speed $\overline{U}$ plotted against parameter β: data taken from Figure 7. Also shown (large symbols) are selected values of ϵ.

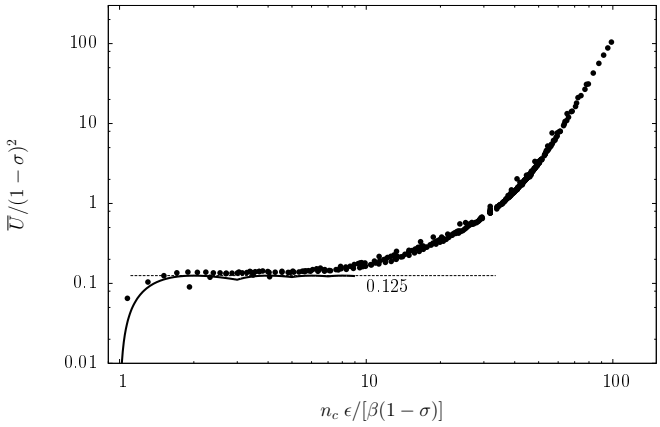

Figure 9: Rescaled incremental propagation speed $\overline{U}$ (filled symbols) plotted against the rescaled number of unstable wavelengths n_c. Data taken from Figure 7. Bold line, analytical incremental speed U_N Eq. (10).

interchangeably with $\overline{U}$ for ease of notation), where from Eq. (6), the scaling emerges from $u/\tau = (F/t)/(1-\sigma)^2$. This rescaling effectively compensates for the increase in flame perturbation amplitude as the thermal expansion increases. Thus, any effect of thermal expansion (and thus on corrugation amplitude) on the propagation speed is factored out, leaving the effect of the extent of flame corrugation, measured by parameter β. Being the critical wavelength λ_c' a single-valued function of β, as shown in Fig. 2(b), the collapsed incremental propagation speed data of Fig. 8 can be equivalently recast as a function of $\lambda_c' = \lambda_c\beta(1-\sigma)/\epsilon$. However, a more effective measure of the extent of corrugation than λ_c is the parameter $n_c = L/\lambda_c$ which measures the number of unstable wavelengths in the domain L. We can therefore recast Fig. 8 as a function of the rescaled number of unstable wavelengths $n_c\epsilon/[\beta(1-\sigma)]$, thus obtaining Fig. 9. We note that for $\beta \ll 0$ (corresponding to low values of $n_c \to 1$) the scaling function $\epsilon/[\beta(1-\sigma)] \approx 1$ so that for purely hydrodynamically unstable (thermodiffusively stable) flames, the rescaled and the actual values of n_c effectively coincide. When $\beta \gg 0$ (corresponding to values of $n_c \gg 1$), the scaling function is well above unity so that for thermodiffusively unstable flames the rescaled values of n_c are substantially larger than the actual values and the scaling function effectively operates a stretching transformation on n_c.

In conclusion, Fig. 9 shows that a universal scaling law can be recovered between the incremental propagation speed U and the number of unstable wavelengths n_c when both are suitably rescaled by means of scaling functions which only depend on the thermophysical parameters σ and ϵ. In the context of the simplifying assumptions of the Sivashinsky model, such scaling functions are lacking a factor expressing the dependence of the transport coefficients on temperature. This would imply a modified fourth order derivative term in (1) requiring the extension of the dispersion relation (8) to the stabilizing fourth order term, which as mentioned was never done in the literature. Nevertheless, our result will prove a useful guideline in the search of a scaling behavior for actual flames, as illustrated in section 3. Indeed $n_c = L/\lambda_c$ is a parameter which can be readily recovered for any realistic configuration, being L a measure of

the largest characteristic hydrodynamic length and λ_c a function of the nature and composition of the flammable mixture as well as the ambient pressure.

The particular form of the scaling law displayed in Fig. 9 can be explained in terms of the following arguments. When $\beta < 0$ the flame exclusively experiences hydrodynamic instability and this generally results in the formation of a single cusp-like flame shape pointing towards the burned gas, that propagates at a constant speed. Figure 8 shows that such speed has the asymptotic value of $U/(1-\sigma)^2 = 0.125$ which is attained as $\beta \to -\infty$. This coincides with the limiting configuration of a pole solution of Eq. (4), which exists only for $\epsilon = -1$, with increasingly large number of poles, as observed in [1]. The analytical expression of the incremental increase in propagation speed, for an N-pole solution [42, 1] of Eq. (4), reads $U_N = 2\pi\alpha N(1 - 4\pi\alpha N)$ and indeed plateaus at the value of 0.125 for large N, i.e. sufficiently small α, where $N = \mathrm{Int}\left[\frac{1}{8\pi\alpha} + \frac{1}{2}\right]$. From the dispersion relation corresponding to Eq. (4), it can be shown that $n_c = 1/(4\pi\alpha)$, so that $N = \mathrm{Int}\left[\frac{n_c}{2} + \frac{1}{2}\right]$ where $n_c = L/\lambda_c$ is the number of unstable wavelengths in the domain L and ultimately

$$U_N = \frac{1}{2}\frac{N}{n_c}\left(1 - \frac{N}{n_c}\right). \tag{10}$$

The function U_N is displayed in Fig. 9 along with the rescaled data and seems to capture the scaling behavior up to some threshold value of the rescaled n_c. Note that the behavior near the bifurcation value $n_c = 1$, after which the front loses stability, is also well captured because, as stated, the scaling function for small $n_c \to 1$ is close to unity.

As $\beta \to 0^-$, Fig. 8 shows that cusp-like solutions seem to diverge from the limiting pole solution and its corresponding value of $U/(1-\sigma)^2 = 0.125$. Indeed, for large enough domains, the cusp sides, which may be considered as quasi-planar [4], become larger than λ_c and undergo secondary bifurcations with the insurgence of additional corrugation. A mathematical description of the origin of this phenomenon is given in the Appendix, where it is explained in terms of the high sensitivity to external noise of the Sivashinsky equation. A more physical explanation is that for $\beta \lesssim 0$, thermodiffusive effects are only weakly

stabilizing ($\epsilon \lesssim 0$) while thermal expansion effects may be large. As a result, additional cellular structures, due solely to hydrodynamic instability, appear on an otherwise smooth cusp-like conformation, thus increasing the propagation speed above the asymptotic value. Such additional structures, obtained in [17] through two-dimensional direct numerical simulations by increasing the lateral size of the simulated flame, were shown to induce a fractal conformation of the flame surface. Very similar fractal corrugation was also observed with a Sivashinsky-type equation in [43, 1]. The onset of this phenomenon was predicted to occur at $n_c \approx 4.5 - 5$ for extemely low turbulence levels in [1] and reported to occur at $n_c \approx 4 - 4.5$ in [4]. Such values seem to be substantially confirmed in Fig 9.

For $\beta > 0$ thermodiffusive instability becomes active, with cellular structures constantly forming and merging on the surface of the cusp-like flame shape. The propagation speed of the front now becomes a marked function of β and the rescaled n_c. As β further increases, the effect of thermodiffusive instability becomes dominant with the flame surface exhibiting a growingly cellular structure. At sufficiently high values of β ($\gg 1$) the hydrodynamic expansion dissappears and the purely thermodiffusive behavior is recovered. In this regime the propagation speed is found to scale approximately as $\sim \beta^3$. This regime is also clearly visible in Fig. 9 as a function of the rescaled n_c which, in this regime, are higher than the actual values of n_c.

2.4. Flame surface density

The Sivashinsky model can be used to extract statistical information on a variety of quantities related to flame morphology. One such quantity, relevant to reaction rate modeling in premixed turbulent combustion is the concept of flame surface density (FSD) Σ. The context of the Sivashinsky model clearly restricts the analysis to a flamelet assumption so that an adequate representation of Σ can be assumed as that originally given by Bray et al. [44]. Given solutions such as those shown in Fig. 4, one can assume flame sheets dividings an unburned zone, identified by progress variable $c = 0$, from a burned zone $c = 1$. The flame

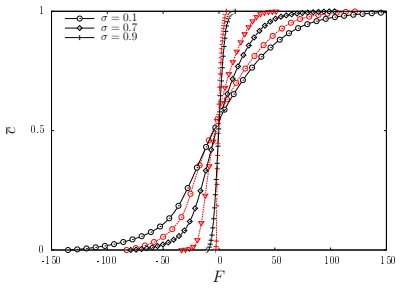

Figure 10: Average progress variable $\overline{c}$ along the vertical flame displacement direction. for $\epsilon = -0.5$ (red dashed lines) and $\epsilon = 0.5$ (black continuous lines) at selected values of σ.

brush will be identified by the mean progress variable $\overline{c}$ along the vertical flame displacement direction. Figure 10 displays the mean progress variable in the vertical direction and clearly shows, as expected, that the flame brush thickness tends to increase as the thermal expansion increases. We also note that flame brushes are generally thicker for $\epsilon > 0$ due to the additional wrinkling of thermal diffusive instabilities.

Flame surface density can be represented [44] as $\Sigma = n_F/\sigma_F$ where n_F is the average number of flame crossings per unit flame length along a constant $\overline{c}$ iso-surface and σ_F is the cosine of the angle between the flame and such iso-surface. Figure 11(a) shows Σ as a function of the mean progress variable for two values of ϵ and several thermal expansion coefficients. Flames exhibiting thermal diffusive instabilities ($\epsilon = 0.5$) also exhibit larger flame surface densities. While this is essentially due to the extra small scale wrinkling of thermal diffusive nature, caution must be adopted when analyzing such results as the Sivashinsky model constrains flame displacement F to be a single valued function of x. On the other hand, real flames may exhibit folds or pockets which can drastically influence both their flame surface density and propagation speed. Given a flame brush, a measure of the underlying flame wrinkling is given by the wrinkling factor [45], defined as $\Xi = \Sigma/|\nabla\overline{c}|$ where the gradient is intended in the vertical displacement direction. Again, the largest flame wrinkling is shown by flames exhibiting thermal diffusive instabilities ($\epsilon = 0.5$).

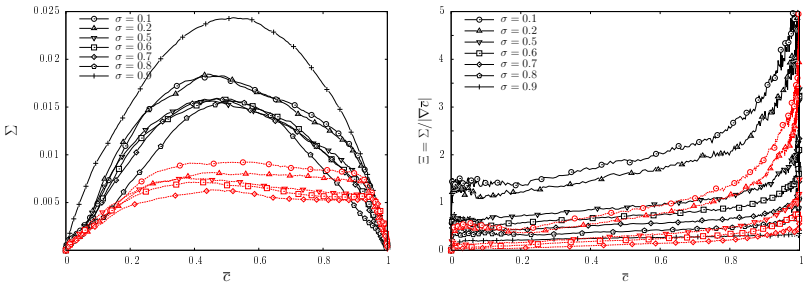

(a) (b)

Figure 11: (a)Flame surface density $\Sigma = \overline{|\nabla c|}$ (b) Wrinkling factor $\Xi = \Sigma/|\nabla\overline{c}|$, for $\epsilon = -0.5$ (red dashed lines) and $\epsilon = 0.5$ (black continuous lines) at various values of σ.

2.5. Hydrocarbon and hydrogen mixtures.

Asymptotic hydrodynamic theory, such as that presented in [38] and yielding the dispersion relation Eq. 8, can be utilized to estimate the location, within the $(\epsilon, 1-\sigma)$ plane, of actual fuel/air mixtures at variable equivalence ratios. Using a procedure similar to [13, 2] and mixture data from various sources, one obtains the results displayd in Fig.12. Clearly, only a small subdomain of the plane is effectively spanned by actual fuel/air mixtures. Fig.12 also clearly shows that the $\epsilon > 0$ zone, where thermal-diffusive instabilities are active, can be accessed only by hydrogen/air mixtures. As demonstrated by data from Ref.[25], shown in Fig.12, a dual-fuel mixture of propane and hydrogen in air can also access the $\epsilon > 0$ zone, provided the relative abundance of hydrogen is large enough.

The diagram of Fig.12 proves effective in locating the stability properties of premixed flames of various mixtures. Indeed, given a mixture composition, the location on such diagram can be identified, revealing both the potential presence of thermodiffusive effects and the extent of thermal expansion (hydrodynamic) effects. Points corresponding to recent DNS simulations, including those presented in the present study, are also located on the diagram. A further analysis, based either on hydrodynamic theory and Eq. 8 or on the numerical recontruction via direct numerical simulation (DNS) of dispersion relations, can reveal, for each flame, the cut-off wavelength λ_c and thus the number of unstable

wavelengths $n_c = L/\lambda_c$ for a given domain size or characteristic hydrodynamic length L. This will prove useful, as illustrated in the following section, in extracting possible universal characteristics in the propagation of unstable flames, similarly to those observed in Fig. 9 for the Sivashinsky model.

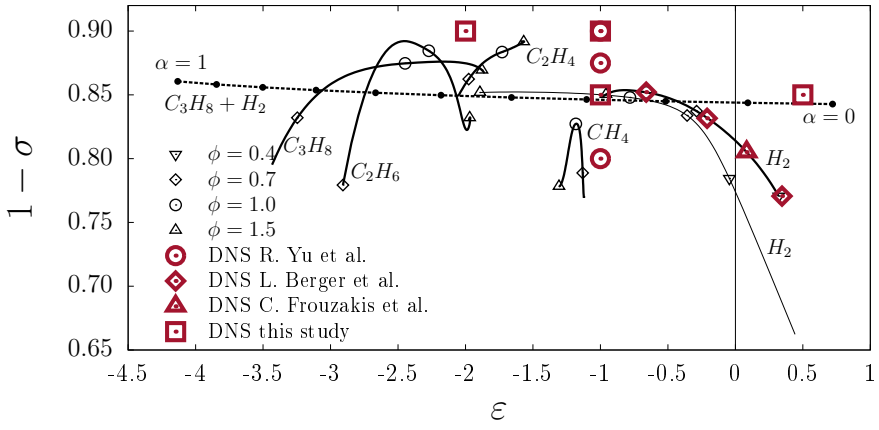

Figure 12: Locus of $(\epsilon, 1-\sigma)$ points for flammable mixtures at variable equivalence ratio ϕ or mixing ratio α. Values of the critical Lewis number Le_0 are estimated via eq.(9 with temperature independent properties. Bold continuous lines: hydrocarbon/air and hydrogen/air mixtures at variable ϕ where Le is an effective Lewis number taken as a weighted average of individual Le numbers of oxidixer and fuel [38, 46] and functions $\sigma(\phi)$ and $Ze(\phi)$ are fitted from experimental data by Tseng [47]. Thin continuous line: similar hydrogen/air mixture with data fitted from Ref.[48]. Dashed bold line: data from Ref.[25] relative to a dual-fuel hydrogen-propane mixture in air at $p = 5$ atm and at an overall eqivalence ratio $\phi = 0.8$, the "mixing ratio" α measuring the relative proportion of the two fules ($\alpha = 0$ being pure hydrogen and $\alpha = 1$ pure propane). Bold red symbols indicate current and literature DNS simulations.

3. DNS of unstable flames

In this section we move away from the weakly nonlinear Sivashinsky model and its limiting assumptions and utilize direct numerical simulations to analyze, in a more realistic setting, the behavior of intrinsically unstable, nominally planar flames. In particular, simulations are performed for a set of parameters that

inhibit as well as promote thermal diffusive instabilities, thereby allowing the analysis of their interaction with the ubiquitous hydrodynamic instabilities. We draw from the findings of the Sivashinsky model and especially from the general scaling of the rescaled propagation speed illustrated in Fig. 9 as a function of the rescaled parameter n_c, in order to verify if a coherent behavior persists in the context of, finite thickness, generic morphology flame fronts at arbitrary density ratios and Lewis numbers.

3.1. Description of DNS simulations

In the present study a well established numerical framework for the direct simulation of intrinsic flame instabilities is employed [2, 49, 16, 50]. Such framework is based on the low-Mach number approximation of the governing equations and on the transport of temperature and a deficient reactant, which govern the reaction rate of a one-step irreversible reaction. The mentioned approach is implemented in an equation-of-state-independent version [51, 52, 53, 54, 55] of the incompressible and variable density massively parallel flow solver *nek5000* [56] which is based on the spectral element method (SEM) [57] for the discretization of the governing equations.

A set of two dimensional simulations of unstable, planar flames are carried out consisting in two series of flames, denoted by suffix TD (thermal-diffusive) and DL (Darrieus-Landau) depending on the destabilizing or stabilizing character of thermal-diffusive effects respectively. Each series consists of three simulations, characterized by increasing values of n_c which is obtained via the numerical evaluation of the cut-off lengthscale λ_c as done for instance in [16]. The computational setup is an inflow/outflow configuration [58] characterized by periodic boundary conditions in the crosswise direction which is also taken as the reference hydrodynamic length L. In the streamwise direction, the dimension of the domain is chosen in order to correctly contain the flame for the entire nonlinear evolution studied. The computational domain is uniformly discretized using square spectral elements obtaining at least $\sim$ 14 grid points, for each flame, within the thermal thickness δ_T of a corresponding 1D unstretched freely

Sim.	ϵ	$1-\sigma$	Le	n_c	L/ℓ_D	S_w/S_L
DL1	-2.0	0.90	1.36	9.2	400	1.57
DL2	-1.0	0.85	1.00	13.7	400	1.32
DL3	-1.0	0.90	1.00	16.3	400	1.85
TD1	0.5	0.85	0.49	7.6	40	2.03
TD2	0.5	0.85	0.49	20.0	105	4.03
TD3	0.5	0.85	0.49	76.0	400	4.52

Table 1: Summary of DNS simulations of purely hydrodynamically (DL) or thermodiffusively (TD) flames. $Ze = 8$ for all simulations.

propagating flame, defining the thermal thickness as $\delta_T = (T_b - T_u)/\max(\nabla T)$. The initial conditions are generated extrapolating over the periodic direction 1D flame profiles with the addition of a small broadband velocity disturbance to trigger the instabilities and promote the onset of the non-linear regime. After reaching the non-linear regime, the simulations are carried for at least 100 laminar flame times in order to collect statistical results.

A summary of the relevant parameters for the six performed simulations is given in Table 1. Note that thermodiffusively stable flames (DL), which exhibit purely hydrodynamic instabilities, have markedly larger values of λ_c in units of flame thickness. This results in a range of values of n_c that can be explored by the DL series using similar computational resources, is clearly narrower than the TD series. Figure 13 shows instantaneous realizations of the non dimensional temperature fields in the non-linear regime.

Observing the TD series at the top of Fig. 13 as n_c increases from left to right, we notice increasing corrugation which dramatically alters the flame morphology. A ubiquitous small scale corrugation, seemingly of constant scale in units of flame thickness, is superimposed, for a large enough n_c, on finger-like, large scale structures (flame fingers). The small scale corrugation is observed to convect along the sides of the flame fingers due to a tangential component of the flow velocity, while the asymmetric fingers exhibit a lateral motion, inducing

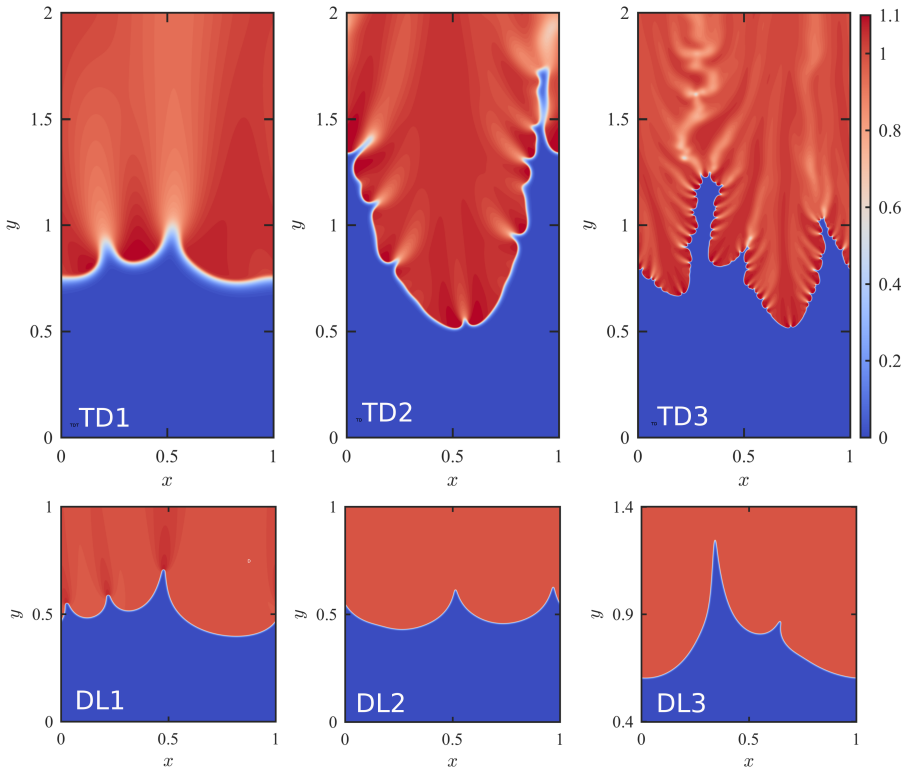

Figure 13: Instantaneous non dimensional temperature fields for the two-dimensional DNS simulations of Tab. 1.

their periodic coalescence. This confirms the characteristic patterns observed by Berger et al. in [18] for two-dimensional DNS of lean hydrogen flames. In their study, the small scale corrugation was observed to be of the same size of the most amplified wavelength as calculated from a numerically derived dispersion relation. The large scale, finger-like corrugation, on the other hand, was observed only for large enough domains and no further scale of larger size was observed for yet larger domains. This domain independence of spatial scales is also confirmed by the present study as discussed later.

Contrary to solutions of the Sivashinky equation, the flame sheet of the TD series now exhibits multiple folds which were previously inhibited. This clearly suggests that the Sivashinky equation is expected to be a poor model of thermodiffusively unstable flames. Sub-adiabatic temperatures downstream of the flame are also visible, indicating the tendency of flame breakup, typical of sub-unity Lewis numbers. The substantial drop in temperature here is not associated with flame extinction because, as noted in [59, 60], in adiabatic systems, despite the reduced reaction rate, the unburned reactant gets completely consumed. The DL1 simulation, for which $Le > 1$, on the contrary, exhibits super-adiabatic temperatures.

The three simulations of the DL series clearly exhibit the characteristic large size cusp-like corrugation, reminiscent of "pole solutions" described earlier, with smaller size corrugation appearing on the cusp sides. For large enough values of n_c, this secondary corrugation was observed to eventually become fractal [17], although in the DL1-3 series n_c seems to still be excessively small to achieve such transition. We note in passing that such fractal conformation is a feature of extremely large scale flames, for which L/ℓ_D may exceed values of say 10^3. For equivalent turbulent flames, subject to turbulent fields characterized by integral length scales of the order of L, it is likely that the Kolmogorov scale may be considerably larger than the flame thickness, driving the Karlovitz number to unrealistically low values, hardly observed in practical devices.

3.2. Flame surface density

Similarly to the Sivashinsky model, we can extract statistical quantities from the DNS data such as the mean progress variable $\bar{c}$ along the vertical direction, the flame surface density $\Sigma = \overline{|\nabla c|}$ and the wrinkling factor $\Xi = \overline{|\nabla c|}/|\nabla \bar{c}|$. Such quantities are shown in Figures 14-16. In particular, Fig. 14 shows wider flame brushes as n_c increases, which highlights, as expected, a more intense corrugation as the number of unstable wavelengths in the domain increases. Figure 15 displays the flame surface density, defined as $\Sigma = \overline{|\nabla c|}$, conditioned to the mean progress variable. Generally, Σ is observed to decrease as n_c increases, essentially due to a wider flame brush which reduces the flame surface density. In the $Le < Le_0$ (TD) case, a peak of Σ is observed towards the fresh mixture. Observing Fig. 13, this is attributed to the presence of finger-like structures (TD2-3) protruding towards the fresh mixture, observed in other simulations [18] and experiments [61]. In addition, the wrinkling factor shown in Fig. 16, confirms the trend observed in the Sivashinsky model with the wrinkling factor being larger for $Le < Le_0$ flames which exhibit additional wrinkling of thermodiffusive nature. Finally, while some degree of similarity can be observed for the $Le > Le_0$ cases between the DNS and the Sivashinky results, severe differences arise in the $Le < Le_0$ cases, where thermodiffusive effects strongly wrinkle and distort the flame to an extent not predictable by a weakly nonlinear model.

3.3. Propagation speed

The Sivashinsky model revealed (see Fig. 9) a universal behavior of the incremental propagation speed U of a corrugated flame front as a function of n_c when both are adeguately rescaled according to functions depending on thermochemical parameters. This observation, ultimately due to the one parameter reformulation of the Sivashinky model Eq. (5)-(6), should clearly not be generalized to real flames as it is gleaned in the context of a weakly nonlinear model for which flame perturbations are small and single valued, thus excluding any flame fold or pocket which may drastically alter such scenario. Nevertheless,

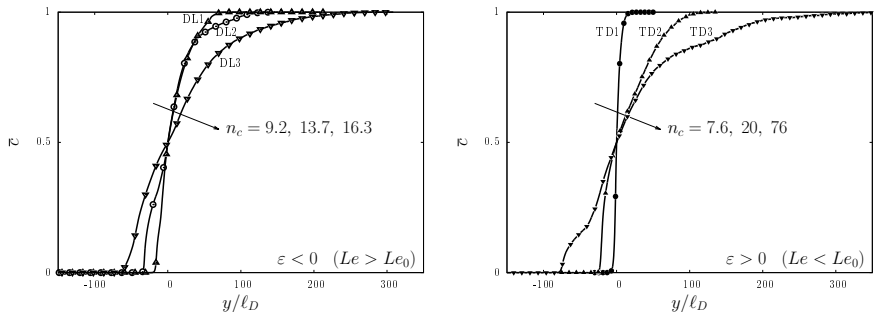

(a) (b)

Figure 14: Mean progress variable $\overline{c}$ as a function of vertical direction y, measured in units of flame thickness ℓ_D for (a) $Le > Le_0$ (DL) flames; (b) $Le < Le_0$ (TD) flames.

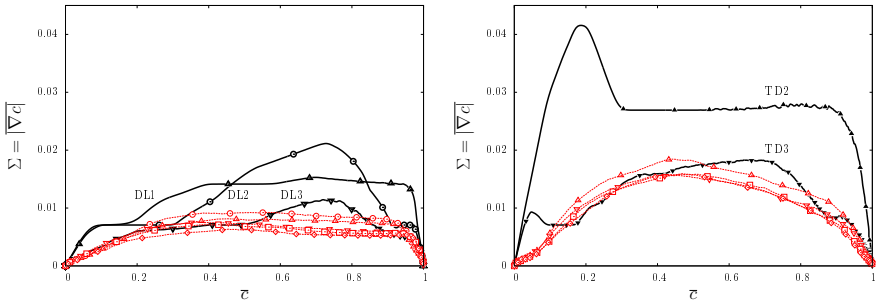

(a) (b)

Figure 15: Flame surface density $\Sigma = \overline{|\nabla c|}$ conditioned to mean progress variable for $\overline{c}$ for (a) $Le > Le_0$ (DL) flames; (b) $Le < Le_0$ (TD) flames. Red lines correspond to the Sivashinsky model.

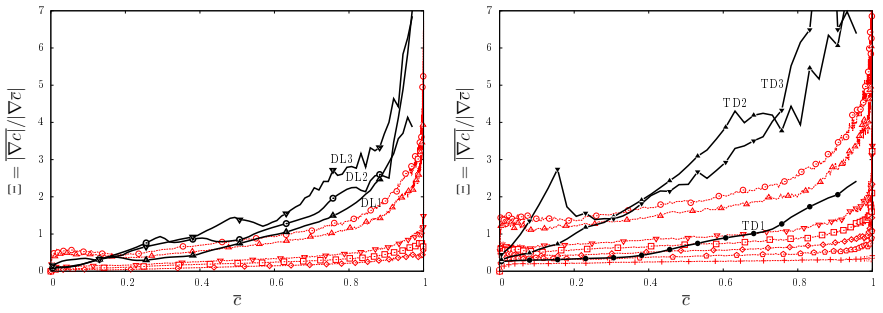

(a) (b)

Figure 16: Wrinkling factor $\Xi = \overline{|\nabla c|}/|\nabla \overline{c}|$ conditioned to mean progress variable for $\overline{c}$ for (a) $Le > Le_0$ (DL) flames; (b) $Le < Le_0$ (TD) flames. Red lines correspond to the Sivashinsky model.

it appeared clear that thermal expansion σ plays a role in modulating the amplitude of flame corrugation and thus in affecting the incremental propagation speed U. Thus the rescaling of U with respect to an adequate function of the thermal expansion coefficient should serve the purpose of filtering out such effect leaving only the effect of the extent of flame wrinkling. The latter was taken into account through parameter n_c, again suitably rescaled by a function which, at least for low values of n_c was noticed to be close to unity. We conclude that a universal scaling law of the kind shown in Fig. 9 can be formally represented as $U/U_m(\sigma) = f[n_c\, U_n(\epsilon, \sigma)]$, where U_m and U_n are generic scaling functions.

Following such guidelines, we can tentatively propose a general form for the scaling law of the nondimensional incremental flame speed U_w of a generic real flame as follows:

$$\frac{S_w}{S_L} - 1 = U_w(\sigma, n_c) = U_m(\sigma) f(n_c) \tag{11}$$

where S_w is the dimensional corrugated flame speed. Note that this scaling law, while formally similar to the Sivashinsky type, is structurally simpler as no scaling is envisioned for the variable n_c, effectively placing $U_n = 1$. This will operate no stretching of the variable n_c, which in Fig. 9 was rather intense for thermodiffusively unstable flames ($\beta > 0$), i.e. at high values of n_c. Such choice

is grounded on simplicity and on the lack of a clear form for U_n applicable to real flames. This may suggest that thermodiffusively unstable flames may scale differently as a function of n_c than purely hydrodynamically unstable flames, something that anyway clearly emerged from the morphological differences of TD and DL simulations of Fig. 13.

In [62], in the context of an evolution equation model for a hydrodynamically unstable front, an expression for the scaling function $U_m(\sigma)$ was derived for realistic values of the thermal expansion coefficient. The incremental propagation speed of a steady corrugated front was expressed [62, 17] by Eq. 11 where $f(n_c)$ coincides with the analytical function U_N of Eq. 10. The scaling function $U_m(\sigma)$ can be verified directly through DNS by computing the incremental flame speed $U_w = (S_w/S_L) - 1$, for various values of σ, of a set of hydrodynamically unstable flames which have attained a steady, cusp-like conformation. This was done, until attainment of steady state, by propagating initially perturbed flame fronts at varying σ and constant $n_c = 3$. In other words, each flame is propagated in a domain of lateral size $L = 3\lambda_c$, where λ_c was estimated via dispersion relation Eq. 8 with $Le = 1$ and $Ze = 8$. Results are shown in Fig. 17 which displays flame profiles as representative contours of deficient reactant concentration $Y = 0.5$, together with the analytical function $U_m(\sigma)$ from [62] and the computed values of $U_w/f(n_c = 3)$, which correspond to numerical estimates of the scaling function once, in Eq. 11 it is assumed that $f(n_c) = U_N$ from Eq. 10. As can be observed, the analytical scaling function captures the effect of thermal expansion on the propagation speed with reasonable accuracy.

We now utilize the numerical simulations of Table 1 to verify the scaling proposed in Eq. 11 with the scaling function $U_m(\sigma)$ shown in Fig. 17. The ensuing dataset, however, is insufficient for such task and it is therefore enriched by additional sets of literature data from recent simulations of unstable flames. In particular we used two dimensional simulations by the following groups:

(a) Yu et al [17] of hydrodynamically unstable one-step chemistry flames at $Le = 1$ ($\epsilon = -1$) and $1 - \sigma = 0.8, 0.875, 0.9$ in the range $n_c = 1 - 95$,

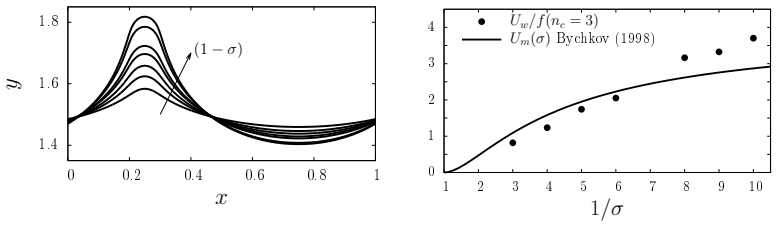

(a) (b)

Figure 17: (a) Steady flame profiles of hydrodynamically unstable flames for which $n_c = 3$ and $(1-\sigma) = 0.5, 0.67, 0.75, 0.8, 0.83, 0.875, 0.9$. Domain is shown in units of L. (b) Continuous line: Scaling function $U_m(\sigma)$ from Bychkov [63]; Filled dots: incremental flame speed $U_w/f(n_c = 3)$ computed from numerical simulations of hydrodynamically unstable flames.

(b) L. Berger et al. [18] of thermodiffusively unstable, lean ($\phi = 0.44$), hydrogen flames at an estimated $Le = 0.39$ ($\epsilon = 0.35$) and $1-\sigma = 0.77$ in the range $n_c = 1-300$,

(c) Frouzakis et al. [64] of lean to rich hydrogen flames which are both hydrodinamically and thermodiffusively unstable ($\phi = 0.5$, estimated $Le = 0.53$ and $1-\sigma = 0.8$) or only hydrodinamically unstable ($\phi = 0.75-2.0$, estimated $Le = 0.82-1.96$ and $1-\sigma = 0.835-0.854$) in the range $n_c = 1-3$.

Results are shown in Fig. 18 where the rescaled incremental propagation speed $U_w/U_m(\sigma)$ for each simulation is reported as a function of the corresponding parameter n_c. An initial observation is that the DNS dataset, when rescaled, seems to roughly collapse onto two distinct scaling behaviors. Indeed, a clear difference exists between the behavior of $Le > Le_0$ (empty symbols) from the $Le < Le_0$ (filled symbols) flames, the latter propagating considerably faster than the former. The existence of two visibly different scaling behaviors for purely hydrodynamically ($Le > Le_0$) and thermodiffusively ($Le < Le_0$) unstable flames, was anticipated earlier and is due to the vastly different morphology. In addition, the lack of an adequate stretching function on the independent parameter n_c prevents the data to collapse on a unique scaling behavior, contrary

to the Sivashinky model.

Purely hydrodynamically unstable flames ($Le > Le_0$) seem to exhibit incremental propagation speeds which follow quite well the analytical incremental propagation speed of pole solutions $U_N(n_c)$ of Eq. 10. This remains true up to $n_c = 6 - 8$, a cut-off value beyond which additional wrinkling appears. This phenomenon is similar in nature to the one originating from an increasing sensitivity to external noise, illustrated in the Appendix for the Sivashinsky model. As mentioned, Yu et al [17] noticed, for growing domain sizes, and thus growing n_c, an increasingly fractal flame conformation which causes the propagation speed to deviate from the analytical asymptotic value $U_N = 0.125$ of the single cusp conformation. For very large values of n_c it is still unclear whether this behavior will eventually become domain independent and plateau at a constant value. Indeed, simulations of $Le > Le_0$ flames, for which λ_c is relatively large ($\lambda_c \sim 10^2 \ell_D$, with ℓ_D the flame thicknesses), which exhibit $n_c > 10^2$ are still excessively computationally intensive, even in two-dimensions, as they would require lateral domains of the order of say $L > 10^2 \lambda_c \sim 10^4 \ell_D$.

Observing Fig. 18 in the presence of thermal diffusive instability ($Le < Le_0$), on the other hand, flames exhibit a different scaling behavior. The intense small scale corrugation and large scale finger-like structures, observable in Fig. 13, which cannot be reproduced within the weakly nonlinear Sivashinsky model, yield incremental propagation speeds which are far larger than the corresponding $Le > Le_0$ cases at the same values of n_c. A growing trend for the incremental propagation speed is also observed as n_c increases which, however, seems to plateau at a cut-off value of $n_c \approx 30$. Indeed Berger et al. [18], while performing simulations of increasingly wider domains, eventually noticed a domain independence with respect to the flame's propagation speed, indicating the existence of a finite-size largest scale corrugation . This behavior seems to be confirmed by the largest of the $Le < Le_0$ DNS simulations presented in this study (TD3).

3.4. Modelling considerations

Ultimately, Fig. 18 suggests that intrinsically unstable flames tend to propagate according to two distinct scaling laws for the incremental speed, depending on the presence of thermal-diffusive instabilities or lack thereof. We can generically represent such laws as $U_w/U_m = \mathcal{F}(n_c)$. The incremental propagation speed was rescaled according to a function $U_m(\sigma)$ in order to compensate for the effect of thermal expansion and this seems to be effective in leaving $n_c = L/\lambda_c$ as the main surviving independent variable in a laminar scenario, λ_c being a purely thermophysical property of the mixture. As a result, the behavior emerging from Fig. 18 may find applications in a FSD-based premixed turbulent combustion model. The interest here is to express the unresolved wrinkling on a large eddy simulation (LES) grid by means of a modeled generalized FSD $\Sigma = \Xi|\nabla\tilde{c}|$, wher Ξ is the wrinkling factor and $\tilde{c}$ the resolved progress variable. Identifying the wrinkling factor Ξ with the self-turbulent propagation speed, $\Xi = S_w/S_L = 1 + U_w$, then Fig. 18 may yield a model for the sub-grid wrinkling as $\Xi(\sigma, n_c) = 1 + U_m(\sigma)\mathcal{F}(n_c)$. Because Ξ would represent the unresolved wrinkling on the LES grid of size Δ, then in this context Δ would replace the role of hydrodynamic length L so that $n_c = \Delta/\lambda_c$. While these remain preliminary suggestions, future studies will be focused on their testing in a a-priori fashion.

4. Conclusions

The self-turbulent propagation of a premixed flame in a quiescent mixture is analyzed. Self-wrinkling arises as a result of two instability mechanisms: the hydrodynamic or Darrieus Landau (DL) and the thermodiffusive (TD) mechanisms. While the DL mechanism is unconditionally unstable, the TD mechanism can be stabilizing or destabilizing. The conditions for which the two forms of instability can coexist are preliminarily studied using the weakly nonlinear Sivashinky equation in terms of thermal expansion σ and parameter ϵ expressing deviations of the Lewis number from a critical value. The parameter range for which both instabilities are present can only be accessed by lean hydrogen

or hydrogen-diluted mixtures. The largest propagation speeds are observed for flames subject to both forms of instability and inducing a large thermal expansion which modulates the amplitude of the corrugation. Through a variable transformation, the propagation speed, adequately rescaled by a function of the thermal expansion coefficient, can be made to collapse on a universal scaling law as the function of the rescaled parameter $n_c = L/\lambda_c$ measuring the number of unstable wavelengths within the lateral domain L.

A database of two-dimensional direct numerical simulations is then presented, consisting in a series of paradigmatic, nominally planar flames exhibiting only DL instability or both DL and TD instability and characterized by varying number of unstable wavelengths n_c. Destabilizing thermodiffusive effects are observed to deeply corrugate the flame on multiple scales, something that could not be observed in the weakly nonlinear model. On the other hand, purely hydrodynamic effects are manifested as cusp-like structures reminiscent of analytical 'pole' solutions to the Sivashinsky equation. Utilizing three additional DNS databases from the literature we suitably rescale the propagation speed data, to account for thermal expansion, and represent it as a function of n_c. Two different scaling behaviors emerge:

(a) flames subject to purely hydrodynamic (DL) instabilities initially scale similarly to analytical 'pole' solutions, with a plateauing behavior, until n_c exceeds a secondary cutoff at which additional wrinkling emerges, significantly increasing the propagation speed with n_c,

(b) flames subject to the additional TD instability mechanism propagate considerably faster than DL flames, owing to the particular multiscale wrinkling, but the propagation speed which initially grows with n_c, plateaus at a cutoff value of n_c, larger than the previous one, at which the largest structures reach their maximum size.

An approach based on flame surface density is proposed in order to model subgrid self-wrinkling in LES, grounded on the gathered DNS data on propagation speed. Future work will be dedicated to testing such model in a a-priori fashion.

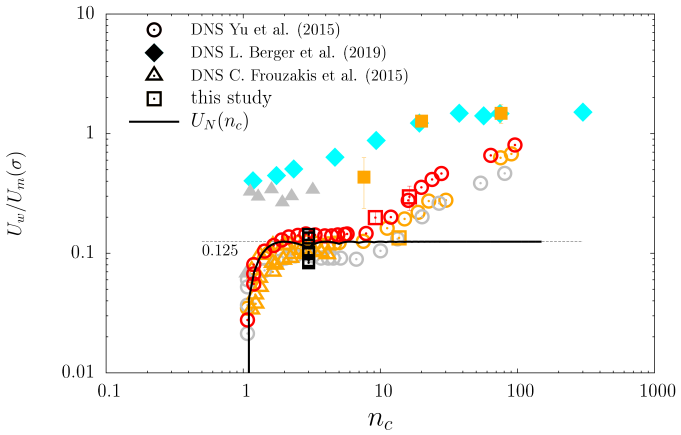

Figure 18: Rescaled incremental propagation speed $U_w/U_m(\sigma)$ as a function of n_c for various DNS studies including the present one. Empty symbols: $Le > Le_0$ ($\epsilon < 0$); filled symbols: $Le < Le_0$ ($\epsilon > 0$). Symbol shape refers to a DNS study while symbol color to thermal expansion. Circles: Yu et. al Ref. [17]; Diamonds: Berger et al. Ref. [18]; Triangles: Frouzakis et al. Ref. [64] Squares: present study. Red: $1-\sigma = 0.9$; Orange: $1-\sigma = 0.835-0.854$; Grey: $1-\sigma = 0.8$; Cyan: $1-\sigma = 0.77$. Black squares refer to the Steady flame profiles of Fig. 17(a). Bold line, analytical incremental speed U_N Eq. (10).

Appendix: sensitivity to external noise

In the absence of thermal-diffusive instabilities ($\epsilon = -1$) the Sivashinsky equation reduces to the form Eq. (4) which is well known to possess a family of exact, steadily propagating analytical "pole solutions" [36]. The stability of such solutions was studied by Vaynblat and Matalon [42, 65] who recognized that the only stable pole solution is the so called "coalescent pole solution" $u_N(\xi)$ characterized by having the largest possible number of poles N for a given value of the parameter α and domain size L. It was recognized [1] that the numerical solution of Eq. (4) indeed converges to the corresponding stable pole solution, possessing a cusp-like flame conformation. However, for large enough domain sizes L and/or small enough values of the parameter α, corresponding to a large number of poles N, additional wrinkling was noticed to appear sporadically on the flame surface, disrupting the steady analytical pole solution [1, 43, 33]. This apparently contradictory behavior, is due to the high sensitivity of the Sivashinsky equation to external noise, which can amplify even the smallest numerical round-off errors, provided N is large enough. This behavior was attributed by Karlin [66] to the non-normal character of the eigenfunctions of the linear operator resulting from the linearization about the pole solution. In other words, as the number of poles N increases, such eigenfunctions, or a subset of them, become increasingly collinear.

More specifically, perturbing the solution about a coalescent N-pole solution, we express the solution as $u(\xi,t) = u_N(\xi) + \phi(\xi,t)$ which, once substituted into Eq. (4) and upon linearizing yields

$$\phi_t = I(\phi) + \alpha\phi_{\xi\xi} - (u_N)_\xi \phi_\xi = \mathcal{A}_N\ \phi \tag{12}$$

where $\mathcal{A}_N$ is the formal expression of the linear operator about the N-pole solution. The linear stability of pole solutions and thus the eigenvalues and eigenfunctions of $\mathcal{A}_N$ were determined analytically in [42, 65] where they were divided into two categories: type I and type II. In particular, type I eigenfunctions were subdivided into symmetric and antisymmetric functions.

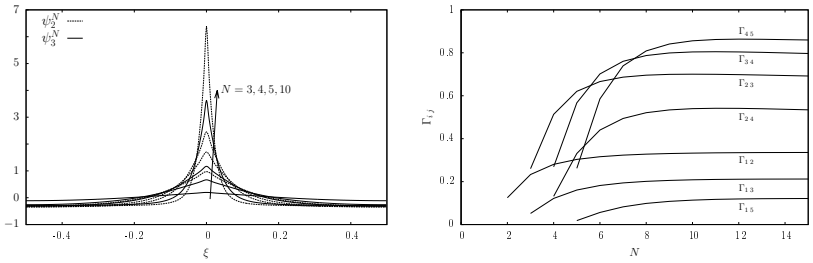

(a) Eigenfunctions of $\mathcal{A}_N$ (b) Inner product $\Gamma_{i\,j}$

Figure 19: Non-normal behavior of Eq. (4).

A rigorous analysis of the non-normal character of $\mathcal{A}_N$ requires the computation of its pseudospectra [67], a concept based on the norm of the resolvent matrix. We can, however, analyze the individual eigenfunctions of $\mathcal{A}_N$ to verify if they become increasingly non-orthogonal as the number of poles N increases. Taking as reference the symmetric type I eigenfunctions ψ_k^N on the interval Ω, we can define the inner product $\Gamma_{i\,j} = (1/||\psi_i||)\int_\Omega \psi_i\psi_j d\xi$, so that eigenfuctions are increasingly non-orthogonal as $\Gamma_{i\,j} \to 1$. Figure 19(a) shows two representative eigenfunctions for increasing pole number N, while Fig. 19(b) shows the inner product $\Gamma_{i\,j}$, suggesting that, indeed, a subset of eigenfunctions tend to become increasingly non-normal as N increases.

Acknowledgments

Some of the coauthors were financially supported by the Italian Ministry of University and Research Ministero dell'Istruzione, Università e della Ricerca (MIUR). The authors acknowledge the Italian Super-Computing Interuniversity Consortium CINECA for support and high-performance computing resources, grant IscrB-DNS-LS.

References

[1] F. Creta, N. Fogla, M. Matalon, Turbulent propagation of premixed flames in the presence of Darrieus–Landau instability, Combust. Theor. Model. 15 (2) (2011) 267–298.

[2] F. Creta, R. Lamioni, P. E. Lapenna, G. Troiani, Interplay of Darrieus–Landau instability and weak turbulence in premixed flame propagation, Phys. Rev. E 94 (5) (2016) 053102.

[3] S. Yang, A. Saha, Z. Liu, C. K. Law, Role of darrieus–landau instability in propagation of expanding turbulent flames, Jour. Fluid Mech. 850 (2018) 784–802.

[4] S. Chaudhuri, V. Akkerman, C. K. Law, Spectral formulation of turbulent flame speed with consideration of hydrodynamic instability, Phys. Rev. E 84 (2) (2011) 026322.

[5] G. Damkölher, Der einflußder turbulenz auf die flammengeschwindigkeit in gasgemischen, Z. Elektrochem. 46 (1940) 601–652, (English translation NASA Tech. Mem. 1112, 1947).

[6] N. Peters, Turbulent combustion, Cambridge University press, UK, 2000.

[7] R. Abdel-Gayed, D. Bradley, M. Lawes, Turbulent burning velocities: a general correlation in terms of straining rates, Proc. R. Soc. Lond. A 414 (1847) (1987) 389–413.

[8] J. H. Chen, H. G. Im, Correlation of flame speed with stretch in turbulent premixed methane/air flames, in: Symp. (Int.) Combust, Vol. 27, Elsevier, 1998, pp. 819–826.

[9] A. Lipatnikov, J. Chomiak, Molecular transport effects on turbulent flame propagation and structure, Progr. Energy Combust. Sci. 31 (1) (2005) 1–73.

[10] H. Kobayashi, H. Kawazoe, Flame instability effects on the smallest wrinkling scale and burning velocity of high-pressure turbulent premixed flames, Proc. Combust. Inst. 28 (1) (2000) 375–382.

[11] V. R. Savarianandam, C. Lawn, Burning velocity of premixed turbulent flames in the weakly wrinkled regime, Combust. Flame 146 (1-2) (2006) 1–18.

[12] D. Bradley, M. Lawes, K. Liu, M. S. Mansour, Measurements and correlations of turbulent burning velocities over wide ranges of fuels and elevated pressures, Proc. Combust. Inst. 34 (1) (2013) 1519–1526.

[13] G. Troiani, F. Creta, M. Matalon, Experimental investigation of darrieus–landau instability effects on turbulent premixed flames, Proc. Combust. Inst. 35 (2) (2015) 1451–1459.

[14] C. R. Bauwens, J. M. Bergthorson, S. B. Dorofeev, On the interaction of the darrieus–landau instability with weak initial turbulence, Proc. Combust. Inst. 36 (2) (2017) 2815–2822.

[15] V. Akkerman, V. Bychkov, Velocity of weakly turbulent flames of finite thickness, Combust. Theor. Model. 9 (2) (2005) 323–351.

[16] P. E. Lapenna, R. Lamioni, G. Troiani, F. Creta, Large scale effects in weakly turbulent premixed flames, Proc. Combust. Inst. 37 (2) (2019) 1945–1952.

[17] R. Yu, X.-S. Bai, V. Bychkov, Fractal flame structure due to the hydrodynamic darrieus-landau instability, Phys. Rev. E 92 (6) (2015) 063028.

[18] L. Berger, K. Kleinheinz, A. Attili, H. Pitsch, Characteristic patterns of thermodiffusively unstable premixed lean hydrogen flames, Proc. Combust. Inst. 37 (2) (2019) 1879–1886.

[19] N. Fogla, F. Creta, M. Matalon, Effect of folds and pockets on the topology and propagation of premixed turbulent flames, Combust. Flame 162 (7) (2015) 2758–2777.

[20] N. Fogla, F. Creta, M. Matalon, The turbulent flame speed for low-to-moderate turbulence intensities: Hydrodynamic theory vs. experiments, Combust. Flame 175 (2017) 155–169.

[21] W. Kim, T. Endo, T. Mogi, K. Kuwana, R. Dobashi, Wrinkling of large-scale flame in lean propane–air mixture due to cellular instabilities, Combust. Sci. Technol. 191 (3) (2019) 491–503.

[22] D. Bradley, M. Lawes, K. Liu, S. Verhelst, R. Woolley, Laminar burning velocities of lean hydrogen–air mixtures at pressures up to 1.0 mpa, Combust. Flame 149 (1-2) (2007) 162–172.

[23] V. Molkov, D. Makarov, A. Grigorash, Cellular structure of explosion flames: modeling and large-eddy simulation, Combust. Sci. Technol. 176 (5-6) (2004) 851–865.

[24] Z. Liu, S. Yang, C. K. Law, A. Saha, Cellular instability in $Le < 1$ turbulent expanding flames, Proc. Combust. Inst. 37 (2) (2019) 2611–2618.

[25] C. K. Law, G. Jomaas, J. K. Bechtold, Cellular instabilities of expanding hydrogen/propane spherical flames at elevated pressures: theory and experiment, Proc. Combust. Inst. 30 (1) (2005) 159–167.

[26] C. Almarcha, B. Denet, J. Quinard, Premixed flames propagating freely in tubes, Combust. Flame 162 (4) (2015) 1225–1233.

[27] J. Quinard, G. Searby, B. Denet, J. Graña-Otero, Self-turbulent flame speeds, Flow Turb. Combust. 89 (2) (2012) 231–247.

[28] K. Mukaiyama, S. Shibayama, K. Kuwana, Fractal structures of hydrodynamically unstable and diffusive-thermally unstable flames, Combust. Flame 160 (11) (2013) 2471–2475.

[29] G. Sivashinsky, Nonlinear analysis of hydrodynamic instability in laminar flames—I. derivation of basic equations, Acta Astronaut. 4 (1977) 1177–1206.

[30] G. Sivashinsky, On flame propagation under conditions of stoichiometry, SIAM Jour. Appl. Math. 39 (1) (1980) 67–82.

[31] Y. Kuramoto, Chemical oscillations, waves, and turbulence, Courier Corporation, 2003.

[32] D. Michelson, G. Sivashinsky, Thermal-expansion induced cellular flames, Combust. Flame 48 (1982) 211–217.

[33] M. Rahibe, N. Aubry, G. Sivashinsky, R. Lima, Formation of wrinkles in outwardly propagating flames, Phys. Rev. E 52 (4) (1995) 3675.

[34] S. Gutman, G. Sivashinsky, The cellular nature of hydrodynamic flame instability, Phys. D 43 (1) (1990) 129–139.

[35] Y. Rastigejev, M. Matalon, Nonlinear evolution of hydrodynamically unstable premixed flames, Jour. Fluid Mech. 554 (2006) 371–392.

[36] O. Thual, U. Frisch, M. Henon, Application of pole decomposition to an equation governing the dynamics of wrinkled flame fronts, in: Dynamics of Curved Fronts, Elsevier, 1988, pp. 489–498.

[37] D. Michelson, G. Sivashinsky, Nonlinear analysis of hydrodynamic instability in laminar flames—ii. numerical experiments, Acta Astronaut. 4 (11-12) (1977) 1207–1221.

[38] M. Matalon, C. Cui, J. Bechtold, Hydrodynamic theory of premixed flames: effects of stoichiometry, variable transport coefficients and arbitrary reaction orders, Jour. Fluid Mech. 487 (2003) 179–210.

[39] P. Clavin, P. Garcia-Ybarra, The influence of the temperature dependence of diffusivities on the dynamics, Journal de Mécanique Théorique et Appliquée 2 (2) (1983) 245–263.

[40] C. Altantzis, C. Frouzakis, A. Tomboulides, M. Matalon, K. Boulouchos, Hydrodynamic and thermodiffusive instability effects on the evolution of

laminar planar lean premixed hydrogen flames, Jour. Fluid Mech. 700 (2012) 329–361.

[41] M. Matalon, The Darrieus–Landau instability of premixed flames, Fluid Dynamics Research 50 (2018) 051412 (23pp).

[42] D. Vaynblat, M. Matalon, Stability of pole solutions for planar propagating flames: I. exact eigenvalues and eigenfunctions, SIAM Jour. Appl. Math. 60 (2) (2000) 679–702.

[43] Y. Rastigejev, M. Matalon, Numerical simulation of flames as gas-dynamic discontinuities, Combust. Theory Model. 10 (3) (2006) 459–481.

[44] K. Bray, M. Champion, P. A. Libby, The interaction between turbulence and chemistry in premixed turbulent flames, in: Turbulent Reactive Flows, Springer, 1989, pp. 541–563.

[45] M. Boger, D. Veynante, H. Boughanem, A. Trouvé, Direct numerical simulation analysis of flame surface density concept for large eddy simulation of turbulent premixed combustion, in: Symp. (Int.) Combust, Vol. 27, Elsevier, 1998, pp. 917–925.

[46] J. Bechtold, M. Matalon, The dependence of the markstein length on stoichiometry, Combust. Flame 127 (1-2) (2001) 1906–1913.

[47] L.-K. Tseng, M. Ismail, G. M. Faeth, Laminar burning velocities and markstein numbers of hydrocarbonair flames, Combust. Flame 95 (4) (1993) 410–426.

[48] J. Yanez, M. Kuznetsov, An analysis of flame instabilities for hydrogen–air mixtures based on sivashinsky equation, Phys. Lett. A 380 (33) (2016) 2549–2560.

[49] R. Lamioni, P. E. Lapenna, G. Troiani, F. Creta, Flame induced flow features in the presence of darrieus-landau instability, Flow Turb. Combust. 101 (4) (2018) 1137–1155.

[50] R. Lamioni, P. E. Lapenna, G. Troiani, F. Creta, Strain rates, flow patterns and flame surface densities in hydrodynamically unstable, weakly turbulent premixed flames, Proc. Combust. Inst. 37 (2) (2019) 1815–1822.

[51] P. E. Lapenna, F. Creta, Mixing under transcritical conditions: An a-priori study using direct numerical simulation, Jour. Supercrit. Fluids 128 (2017) 263–278.

[52] P. E. Lapenna, R. Lamioni, P. P. Ciottoli, F. Creta, AIAA-paper 2018-0346.

[53] P. E. Lapenna, Characterization of pseudo-boiling in a transcritical nitrogen jet, Phys. Fluids 30 (7) (2018) 077106.

[54] P. E. Lapenna, G. Indelicato, R. Lamioni, F. Creta, Modeling the equations of state using a flamelet approach in lre-like conditions, Acta Astronaut. 158 (2019) 460–469.

[55] P. Lapenna, F. Creta, Direct numerical simulation of transcritical jets at moderate reynolds number, AIAA Jour. 57 (6) (2019) 2254–2263.

[56] P. F. Fischer, J. W. Lottes, S. G. Kerkemeier, nek5000 web page, http://nek5000.mcs.anl.gov.

[57] A. T. Patera, A spectral element method for fluid dynamics: laminar flow in a channel expansion, Jour. Comput. Phys. 54 (3) (1984) 468–488.

[58] M. Klein, N. Chakraborty, S. Ketterl, A comparison of strategies for direct numerical simulation of turbulence chemistry interaction in generic planar turbulent premixed flames, Flow Turb. Combust. 99 (3-4) (2017) 955–971.

[59] G. Kozlovsky, G. Sivashinsky, On open and closed tips of bunsen burner flames, Theoretical and Computational Fluid Dynamics 6 (1994) 181–192.

[60] L. Kagan, G. Sivashinsky, Incomplete combustion in nonadiabatic premixed gas flames, Physical Review E 53 (6) (1996) 6021–6027.

[61] D. Fernández-Galisteo, V. N. Kurdyumov, P. D. Ronney, Analysis of premixed flame propagation between two closely-spaced parallel plates, Combust. Flame 190 (2018) 133–145.

[62] V. Akkerman, V. Bychkov, Turbulent flame and the darrieus–landau instability in a three-dimensional flow, Combust. Theory Model. 7 (4) (2003) 767–794.

[63] V. V. Bychkov, Nonlinear equation for a curved stationary flame and the flame velocity, Phys. Fluids 10 (8) (1998) 2091–2098.

[64] C. E. Frouzakis, N. Fogla, A. G. Tomboulides, C. Altantzis, M. Matalon, Numerical study of unstable hydrogen/air flames: shape and propagation speed, Proc. Combust. Inst. 35 (1) (2015) 1087–1095.

[65] D. Vaynblat, M. Matalon, Stability of pole solutions for planar propagating flames: Ii. properties of eigenvalues/eigenfunctions and implications to stability, SIAM Jour. Appl. Math. 60 (2) (2000) 703–728.

[66] V. Karlin, Cellular flames may exhibit a non-modal transient instability, Proc. Combust. Inst. 29 (2) (2002) 1537–1542.

[67] L. N. Trefethen, Pseudospectra of linear operators, SIAM Rev. 39 (3) (1997) 383–406.